MACROSCALE CONNECTOME MANIFOLD EXPANSION IN ADOLESCENCE

Bo-yong Park[a], Richard A. I. Bethlehem[b,c], Casey Paquola[a], Sara Larivière[a], Raul R. Cruces[a], Reinder Vos de Wael[a], Neuroscience in Psychiatry Network (NSPN) Consortium[2] , Edward T. Bullmore[c], Boris C. Bernhardt[a]

[a]McConnell Brain Imaging Centre, Montreal Neurological Institute and Hospital, McGill University, Montreal, Quebec, Canada; [b]Autism Research Centre, Department of Psychiatry, University of Cambridge, Cambridge, United Kingdom; [c]Brain Mapping Unit, Department of Psychiatry, University of Cambridge, Cambridge, United Kingdom

Corresponding Authors:

Boris C. Bernhardt, PhD
Multimodal Imaging and Connectome Analysis Lab
McConnell Brain Imaging Centre
Montreal Neurological Institute and Hospital
McGill University
Montreal, Quebec, Canada
Phone: +1-514-398-3579
Email: boris.bernhardt@mcgill.ca

Bo-yong Park, PhD
Multimodal Imaging and Connectome Analysis Lab
McConnell Brain Imaging Centre
Montreal Neurological Institute and Hospital
McGill University
Montreal, Quebec, Canada
Email: bo.y.park@mcgill.ca

[2]A complete list of investigators from the Neuroscience in Psychiatry Network (NSPN) Consortium can be found in the Supporting Information.

ABSTRACT

Adolescence is a critical time for the continued maturation of brain networks, and the current work assessed longitudinal reconfigurations of diffusion MRI derived connectomes in a large sample (n = 208). We identified an expansion of structural network representations in lower dimensional manifold spaces, with strongest effects in transmodal cortices and indicative of an increasing differentiation of these networks from the rest of the brain. Findings were shown to relate to mainly an increase in within-module connectivity and increased segregation during adolescence. Connectome findings were consistent when additionally controlling for regional changes in MRI measures of cortical morphology and myelin, despite reductions in effect sizes. On the other hand, cortical areas showing manifold expansion were found to become more closely embedded with subcortical targets, notably the striatum. Identified networks were also found to harbor genes significantly expressed in both cortical and subcortical regions. Using supervised machine learning with cross-validation, we demonstrated that cortico-subcortical manifold features at baseline and their maturational change predicted measures of intelligence at follow-up. Our findings chart adolescent connectome development and suggest that brain-wide network reconfigurations offer intermediary phenotypes between genetic-microstructural processes and cognitive-behavioral outcomes.

KEYWORDS: adolescence development; structural connectome manifold; transcriptomic analysis; machine learning; cognitive development

SIGNIFICANCE STATEMENT

We explored how whole-brain structural networks reconfigure during adolescence, using a novel analysis that simultaneously interrogates network and regional features. Our approach revealed an increasing differentiation of the connectome during this critical period, particularly in higher-order prefrontal and parietal regions. We could show that while this effect was only partially related to developmental trajectories of intracortical microstructure and morphology, but rather to changes in connectivity to subcortical areas, particularly the striatum. Cortico-subcortical network effects were also supported by transcriptomics and phenotype prediction, which suggested that cognitive function in adulthood was most effectively predicted when combining cortical and subcortical features. Our findings shed new light on adolescence and support a key role of cortico-subcortical integration in shaping macroscale structural networks.

INTRODUCTION

Adolescence is a time of profound and genetically mediated changes in whole-brain network organization [1–7]. Adolescent development is important for overall maturation in cognitive and educational functions and brain health more generally, a notion reinforced by the overlapping onset of several neurodevelopmental and psychiatric disorders [8–13]. With increased capacity to carry out longitudinal studies in large samples, it is now possible to track changes in brain network organization within subjects, providing mechanistic insights into maturational processes, their biological underpinnings, and their effects on behavior and cognition.

By offering a powerful *in vivo* window into brain organization, neuroimaging techniques such as magnetic resonance imaging (MRI) offer the ability to track adolescent development over time, and to explore associations to cognitive functions. Early cross-sectional and longitudinal studies focused on the analysis of morphological changes [1,2,14–18]. For example, they charted changes in cortical thickness [1,17] and volume measures [2,14,17,19], with initial grey matter increases until late childhood followed by a decline for the rest of the lifespan. More recent work explored changes in intracortical microstructure, capitalizing on myelin-sensitive contrasts such as magnetization transfer ratio (MT) mapping, which generally suggest overall increases in adolescence [20–22] together with depth dependent shifts in intracortical myelin profiles [21]. Several studies suggested connectome reconfigurations in adolescence based on resting-state functional MRI [23,24]. These studies showed that, during development, brain organization is remodeled from a more local towards a more distributed architecture through the relative strengthening of long-range functional connections [23,24]. Collectively, these findings suggest measurable trajectories of intracortical and cortico-cortical aspects of brain organization. Furthermore, studies generally support associations to inter-individual differences and age-related changes in cognitive competences [1,3,25].

Diffusion MRI (dMRI) is a technique sensitive to the displacement of water in tissue and allows for the non-invasive approximation of inter-regional white matter fibers integrity. Prior studies focusing on specific tracts or collections of tracts outlined white matter maturation during development based on dMRI parameters of fractional anisotropy and mean diffusivity [26–31]. Cross-sectional and longitudinal studies have shown changes in the microstructure of major white matter tracts, often characterized by an increased fractional anisotropy and decreased mean diffusivity from childhood to adolescence [26–28,30,32]. These findings have been complemented by assessments of connectome topology using graph-theory [29,30,33]. These studies reported that structural hubs remain relatively consistent across adolescent development [34–40], yet with a continued strengthening of their connectivity profiles that has been related to maturation of long-range association fibers [28–30,32]. The changes in structural connectome organization along continuous axes of the whole-brain during development can be explored using novel manifold learning techniques [41,42], adopted by an increasing literature in adult cohorts. The main idea of these techniques is to project connectome information into low dimensional spaces that capture principal dimensions of whole-brain organization. Offering an alternative and continuous reference frame to study macroscale connectivity, these techniques can visualize salient principles of cortical organization [41,43], and study structure-function coupling [44–46], cognitive processes [47,48], aging effects [49,50] as well as disease-related perturbations [10,51]. In the assessment of adolescent development, manifold learning techniques have recently been applied to show an increasing myeloarchitectural differentiation of association cortex [21], but we lack evidence of how structural connectomes are remodeled in this manifold space during brain development.

The burgeoning imaging genetics field, bolstered by open databases of human transcriptomics [52–55], has illustrated that macroscopic neuroimaging phenotypes can be related to spatial variations at the molecular scale [57] in contexts of healthy brain organization [56,57], brain development [21], and disease [51,58,59]. Combined with a method highlighting developmental time windows [51,55], these approaches provide new insights into spatio-temporal shifts in gene expression that underly imaging and

connectome findings. As such, it is increasingly possible to contextualize macroscopic findings with respect to biological factors and processes, strengthening the role of developmental MRI to bridge molecular factors and indices of cognitive development that are measured using behavioral assays.

Here, we charted adolescent changes in structural connectome organization, based on an accelerated longitudinal neuroimaging study (n = 208) [20,60]. Compared to cross-sectional designs, longitudinal studies track within-subject change, separating developmental effects from between-subject variability [61–65]. Leveraging connectome-wide manifold learning techniques [42], we first estimated longitudinal changes in structural connectome manifolds across age in a compact and lower dimensional analytical space. This approach furthermore allowed for the integration of connectome level findings with changes in MRI-based measures of cortical morphology and proxies of intracortical myelin. Transcriptomic association and developmental enrichment analyses based on post-mortem datasets offered neurobiological contextualization of macroscale connectivity findings, and an exploration of time windows of spatially co-localized gene sets. To explore behavioral associations to our findings, we harnessed supervised machine learning to predict future measures of cognitive function from structural connectome data. Multiple sensitivity analyses were conducted at several steps of our analysis to verify the robustness of our findings.

RESULTS

We studied 208 healthy adolescents and young adults enrolled in an accelerated longitudinal study (48% female; mean ± SD age = 18.82 ± 2.83 years at baseline and 19.95 ± 2.84 at follow-up; inter-scan interval of 11.28 ± 1.96 months) obtained from the Neuroscience in Psychiatry Network (NSPN) 2400 cohort [20,60]. See *Methods* for details on participant selection, image processing, and analysis.

Macroscale structural connectome manifold

A cortex-wide structural connectome manifold, formed by eigenvectors displaying spatial gradients in structural connectome organization, was estimated using non-linear dimensionality reduction techniques for each subject (https://github.com/MICA-MNI/BrainSpace) [42]. Individual manifolds were aligned to a template manifold estimated from a hold-out dataset (see *Methods*) [42]. Three manifold eigenvectors (M1, M2, and M3) explained approximately 50% of variance in the template affinity matrix, with each eigenvector showing a different axis of spatial variation across the cortical mantle (**Fig. 1A**). Eigenvectors depicted a continuous differentiation between temporo-parietal and prefrontal areas (M1), between ventral cortex and somatosensory regions (M2), and between somatosensory and prefrontal cortices (M3). For each participant and time point, we calculated *manifold eccentricity*, a single scalar that calculates the Euclidean distance between the template center and each data point in the manifold space, to simplify the multidimensional manifolds into a single feature. The manifold eccentricity was calculated for all brain regions, and this regional feature was used for assessing overall connectome manifold changes across age in terms of expansion and contraction (**Fig. 1B**) [49].

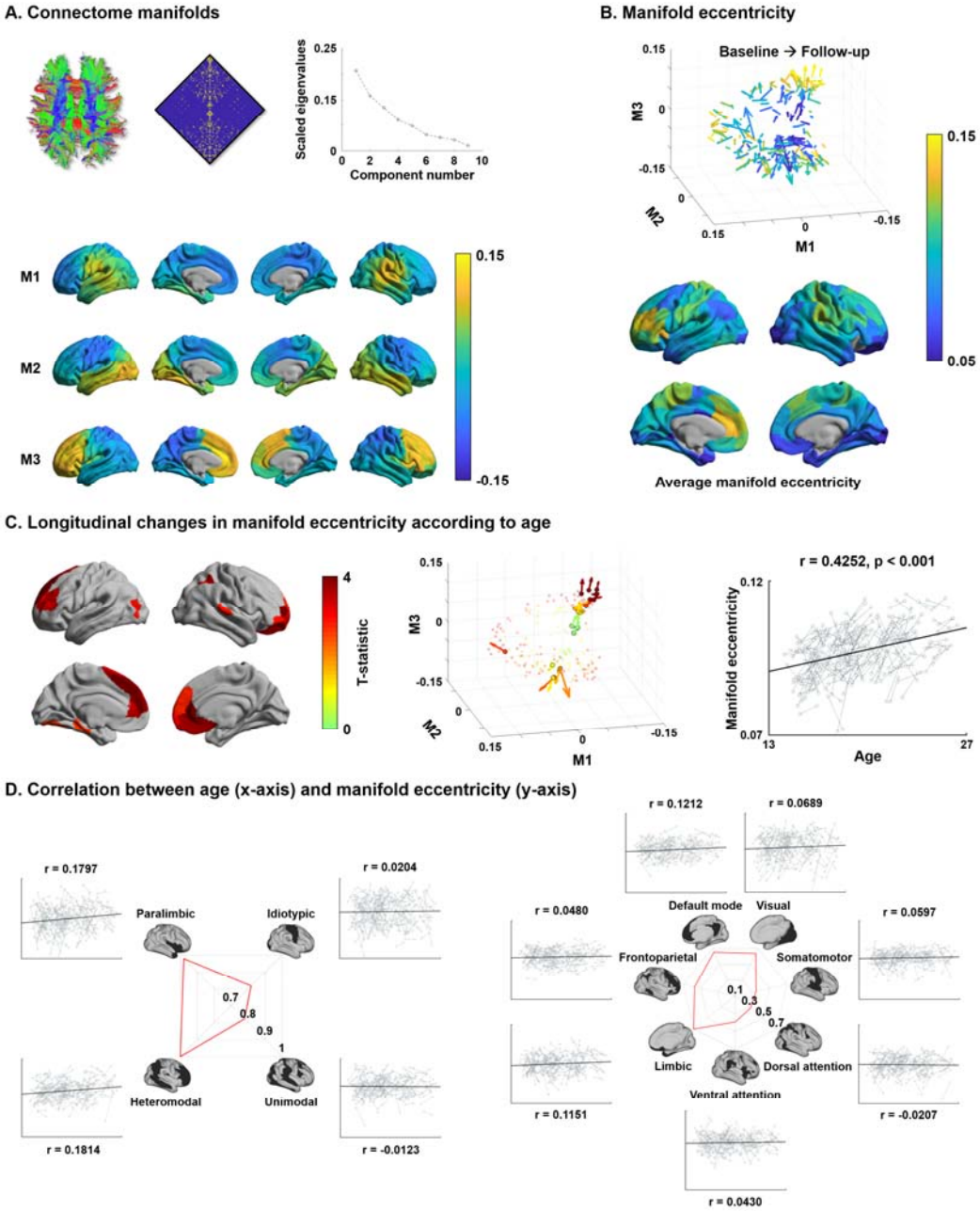

Fig. 1 | Structural connectome manifolds. (A) Systematic fiber tracking based on dMRI generated a cortex-wide structural connectome, which was subjected to diffusion map embedding. As shown in the scree plot, three manifold eigenvectors (M1, M2, M3) explained approximately 50% connectome variance and each depicted a different gradual transition across the cortical mantle. **(B)** Manifold eccentricity measured by Euclidean distance between the template center and each data point. Arrows depict average positional change in connectivity space from baseline to follow-up. The color of each arrow represents each brain region mapped on the surface on the bottom row. **(C)** The t-statistics of regions showing significant longitudinal changes in manifold eccentricity across age, following multiple comparisons correction with a false discovery rate (FDR) procedure. Datapoint colors in the scatter plot represent t-statistics. Identified regions are represented with arrows that originate from baseline to follow-up. Pearson's correlation between age and manifold eccentricity of the identified regions is shown to the right. **(D)** Stratification of age-related changes in manifold eccentricity along cortical hierarchy [66] and functional community [67]. The central radar plots show t-statistics of each hierarchical level or functional community and the scatter plots represent Pearson's correlation between age (x-axis) and manifold eccentricity (y-axis).

Age-related longitudinal changes in manifold eccentricity

Leveraging linear mixed effect models that additionally controlled for effects of sex, site, head motion, and subject-specific random intercepts [68], we assessed longitudinal changes in manifold eccentricity across age (see *Methods*). Manifold eccentricity expanded as age increased, especially in bilateral prefrontal and temporal areas, as well as left early visual and right lateral parietal cortices (false discovery rate (FDR) < 0.05; **Fig. 1C**). Stratifying these effects along four cortical hierarchy levels, defined using an established taxonomy based on patterns of laminar differentiation and tract-tracing data in non-human primates (idiotypic; unimodal association; heteromodal association; paralimbic) [66], we identified peak effects in heteromodal association and paralimbic areas (**Fig. 1D**). Convergent findings were observed when analyzing effects with respect to intrinsic functional communities [67], showing highest effects in default mode and limbic areas followed by visual and frontoparietal cortices. No significant contraction of manifold eccentricity was observed across age.

Association with connectome topology

To conceptualize findings according to topological fingerprints, we correlated manifold eccentricity changes with several graph theoretical measures of the structural connectome [69,70]. We first defined six spatial contiguous clusters within the regions that showed significant age-related changes in manifold eccentricity (see *Fig. 1C*) and plotted cluster-average manifold eccentricity across age (**Fig. 2A**). We then correlated within-subject changes in manifold eccentricity for regions of findings with within-subject changes in degree centrality, connectivity distance, and modular parameters (*i.e.*, within-module degree and participation coefficient based on modules defined via Louvain's community detection algorithm [71]; **Fig. 2B** and **S1**). We found positive associations to degree centrality ($0.21 < r < 0.86$) and within-module degree ($0.17 < r < 0.81$); on the other hand, findings were not consistent for connectivity distance ($-0.09 < r < 0.58$) and participation coefficient ($-0.24 < r < 0.37$). These findings suggest that manifold expansion reflects a concurrent increase of overall connectivity, particularly within modules. Stratifying changes in manifold eccentricity as well as connectome topology measures according to the discretized age bins confirmed these age-related trends (**Fig. S2**). Indeed, except for participation coefficient, values in general increased from childhood to young adulthood.

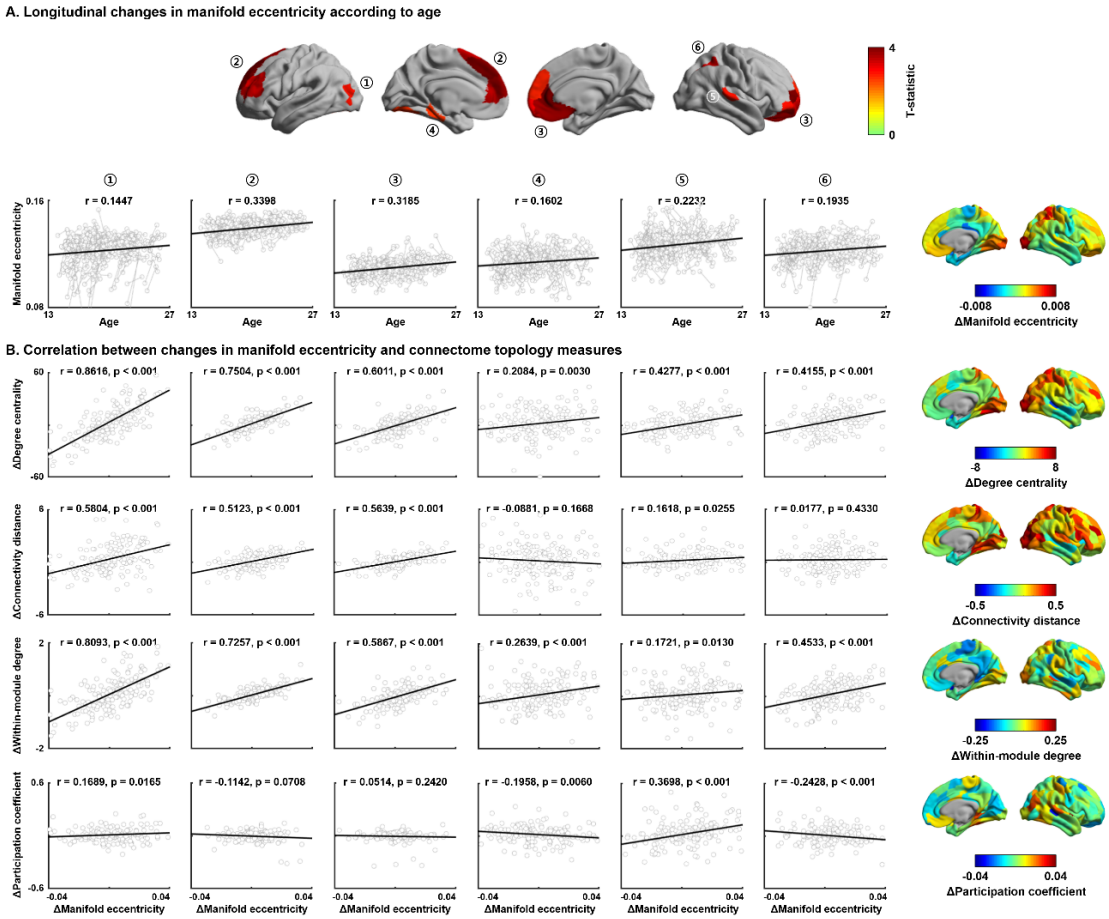

Fig. 2 | Association between structural connectome manifold and connectome topology measures. (A) Six clusters defined within the identified regions that showed significant age-related longitudinal changes in manifold eccentricity (see *Fig. 1C*). Pearson's correlations between age and manifold eccentricity for each cluster are shown on the bottom row. **(B)** Associations between within-subject changes in manifold eccentricity and those of each connectome topology measure. Brain surfaces on the right side represent changes in each measure between baseline and follow-up. Significance was calculated using FDR.

Effects of cortical morphology and microstructure

Previous studies demonstrated significant changes in cortical morphology and microstructure during adolescence, showing co-occurring reductions in cortical thickness and MT skewness, a recently proposed index of depth dependent intracortical myelin changes in multiple lobes [1,2,9,21]. We replicated these findings by showing longitudinal cortical thinning in almost all brain regions across the studied age window ($r = -0.4112$ and $p < 0.001$) as well as reductions in depth dependent MT skewness, suggestive of supragranular enrichment of myelin ($r = -0.4457$ and $p < 0.001$) (**Fig. 3A and S3**). To evaluate whether the age-related changes in manifold eccentricity were robust above and beyond these regional changes in cortical thickness and MT, we implemented linear mixed effect models after correcting manifold eccentricity measures for cortical thickness and MT (**Fig. 3B**). While we observed virtually identical spatial patterns of manifold eccentricity changes in models that controlled for thickness, MT skewness, and both, effects in clusters of manifold eccentricity findings were reduced in models that additionally controlled for these values (average reduction of t-value in models controlling for thickness/MT skewness/both = 42/18/68%).

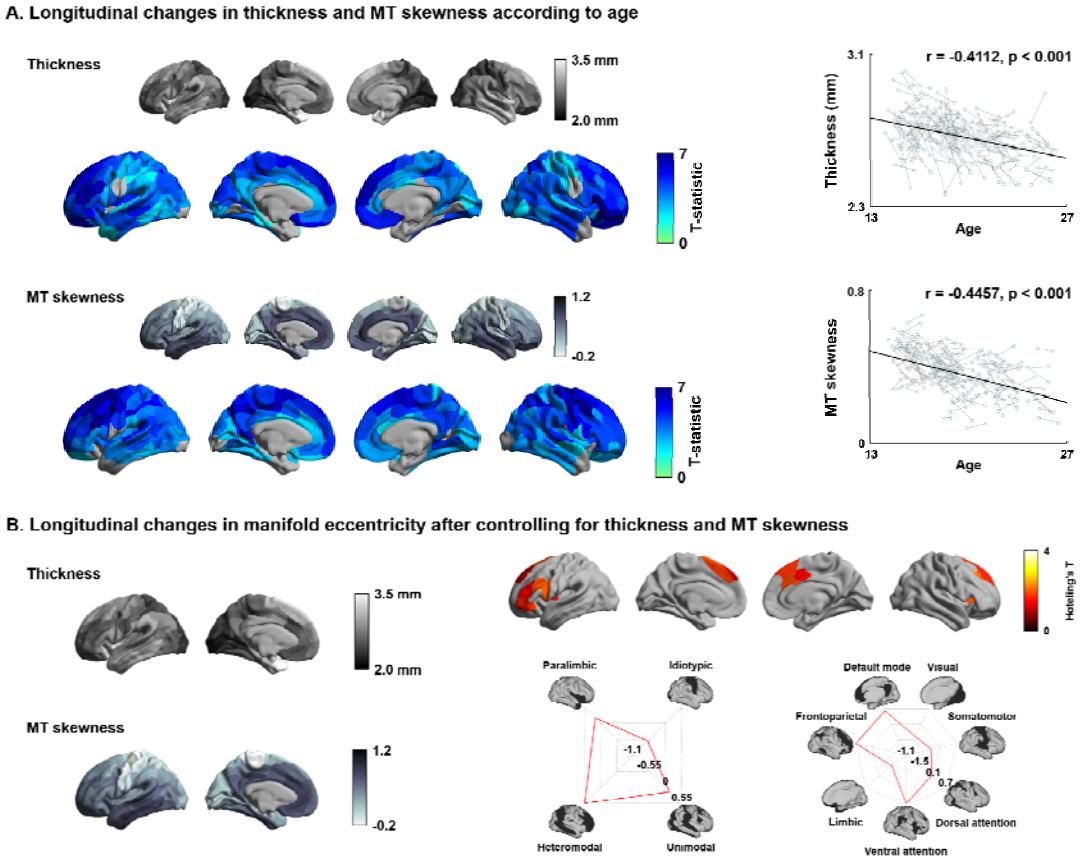

Fig. 3 | Association to morphological and microstructural effects. (A) The t-statistics of identified regions that showed significant age-related changes in cortical thickness (upper row) and MT (bottom row), and corresponding correlation plots with age. Significant decreases are shown in blue. **(B)** Age-related longitudinal changes in manifold eccentricity after controlling for cortical thickness and MT.

Transcriptomic association analysis

Transcriptomic association and developmental enrichment analyses were carried out to contextualize the longitudinal manifold eccentricity changes with respect to patterns of *post-mortem* gene expression from a sample of independent adults (**Fig. 4A**). Specifically, leveraging mixed effect models, we associated the spatial patterns of manifold change across age that controlled for cortical thickness and MT in the NSPN sample with cortical maps of *post-mortem* gene expression data from the Allen Institute for Brain Sciences [52–54]. Among the list of most strongly associated genes (FDR < 0.05), we selected only genes that were consistently expressed across different donors (r > 0.5) [72] (**Data S1**). We fed those into a developmental gene enrichment analysis, which highlights developmental time windows across macroscopic brain regions in which genes are strongly expressed (see *Methods*) [55]. This analysis highlighted marked associations between the spatial pattern of longitudinal change in manifold eccentricity and the expression of genes that were found enriched from childhood onwards in the cortex, thalamus, and cerebellum (FDR < 0.001; **Fig. 4B**). Although genetic signal was reduced, genes were also showing an enrichment for expression in the striatum at the transition from childhood to adolescence (FDR < 0.05). On the other hand, identified genes were not found to be expressed in the hippocampus and amygdala.

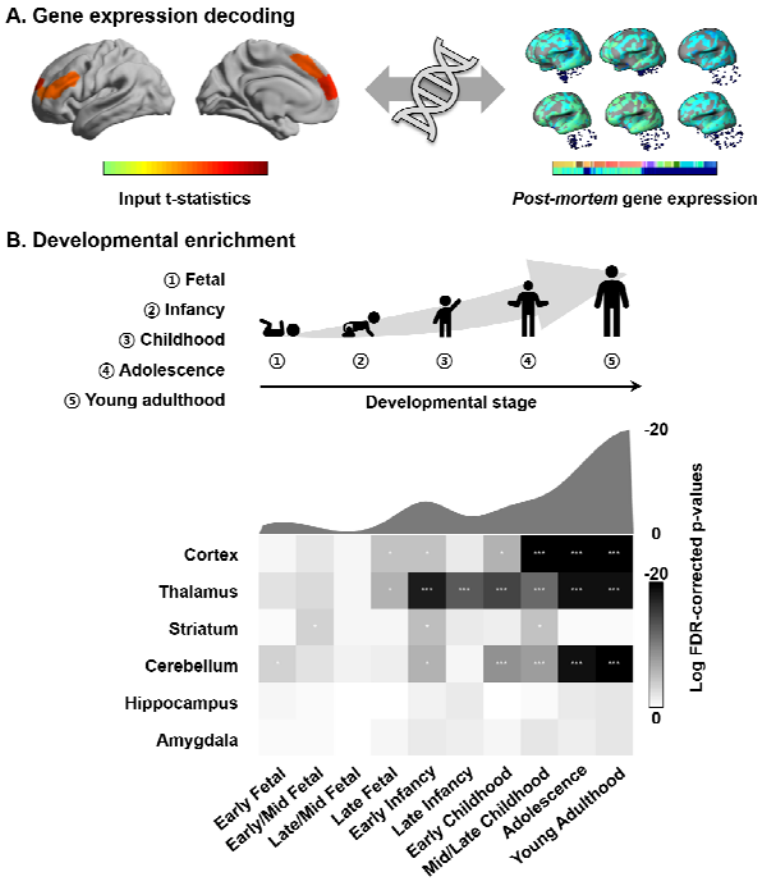

Fig. 4 | Transcriptomic analysis. (A) Gene decoding process by associating t-statistics from the linear mixed effect model with *post-mortem* gene expression maps. **(B)** We identified genes that were spatially correlated with the with input t-statistic map (FDR < 0.05) and selected only those that were furthermore consistently expressed across different donors (r > 0.5). These genes were fed into a developmental enrichment analysis, showing strong associations with cortex, thalamus, striatum, and cerebellum during childhood-to-adulthood time window. The degree of gene expression for developmental windows is reported on the bottom. The curve represents log transformed FDR corrected p-values, averaged across the brain regions reported as on the bottom. ***FDR < 0.001, ** FDR < 0.01, *FDR < 0.05.

Age-related changes in cortico-subcortical connectivity

To assess age-related effects of subcortical nodes, we assessed longitudinal changes in streamline strength between subcortical regions and identified cortical areas (see *Fig. 1C*) across age (see *Methods*). The striatum including bilateral caudate and right putamen, as well as right pallidum, showed significant strengthening of streamlines connecting cortical areas involved in manifold expansion (Pearson's r = 0.2932 and p < 0.001; **Fig. 5A**). Across subcortical nodes, the caudate showed largest changes in streamline strength followed by pallidum and putamen and these regions were significantly correlated with age after correction for multiple comparisons (FDR < 0.05; **Fig. 5B**).

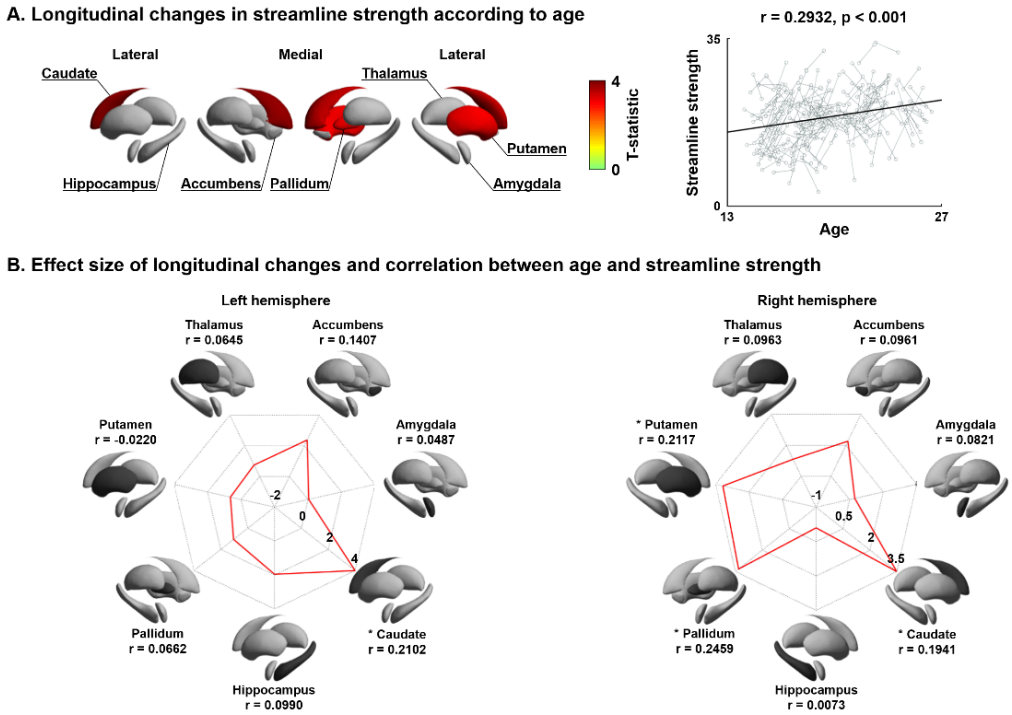

Fig. 5 | Streamline strength between subcortical and cortical regions. (A) The t-statistics of identified subcortical regions that showed significant age-related longitudinal changes in strength of streamlines that connected to identified cortical regions (see *Fig. 1C*). Pearson's correlation between age and streamline strength is shown on the right side. **(B)** Stratification of age-related changes in streamline strength and Pearson's correlation between age and streamline strength along each subcortical region. * FDR < 0.05.

Association between connectome manifold and cognitive function

We utilized a supervised machine learning to predict full intelligence quotient (IQ) at follow-up using manifold eccentricity of the identified cortical regions and streamline strength of the identified subcortical areas that showed significant age-related longitudinal changes. Specifically, we employed elastic net regularization [73] with ten-fold cross-validation (see *Methods*), and repeated the prediction 100 times with different training and test dataset composition to mitigate subject selection bias. The manifold eccentricity of cortical regions at baseline significantly predicted future IQ score (mean ± SD r = 0.2121 ± 0.0252; mean ± SD mean absolute error (MAE) = 8.7646 ± 0.1001), and prediction performance was slightly improved when we combined the manifold eccentricity both at baseline and differences between follow-up and baseline (mean ± SD r = 0.2560 ± 0.0241; mean ± SD MAE = 8.4412 ± 0.1014) (**Fig. 6A**). Notably, prediction accuracy was improved if we considered both cortical and subcortical features (only at baseline: mean ± SD r = 0.2492 ± 0.0299; mean ± SD MAE = 8.8144 ± 0.1712; both at baseline and maturational change: mean ± SD r = 0.3421 ± 0.0231; mean ± SD MAE = 8.5201 ± 0.1572) (**Fig. 6B**). The regions showing strongest predictive validity for IQ were prefrontal, parietal, and temporal cortices, as well as the caudate. The probability map of the selected brain regions (bottom right of *Fig. 6B*) was further decoded using Neurosynth [74], indicating strong associations with higher-order cognitive and social terms (**Fig. S4**).

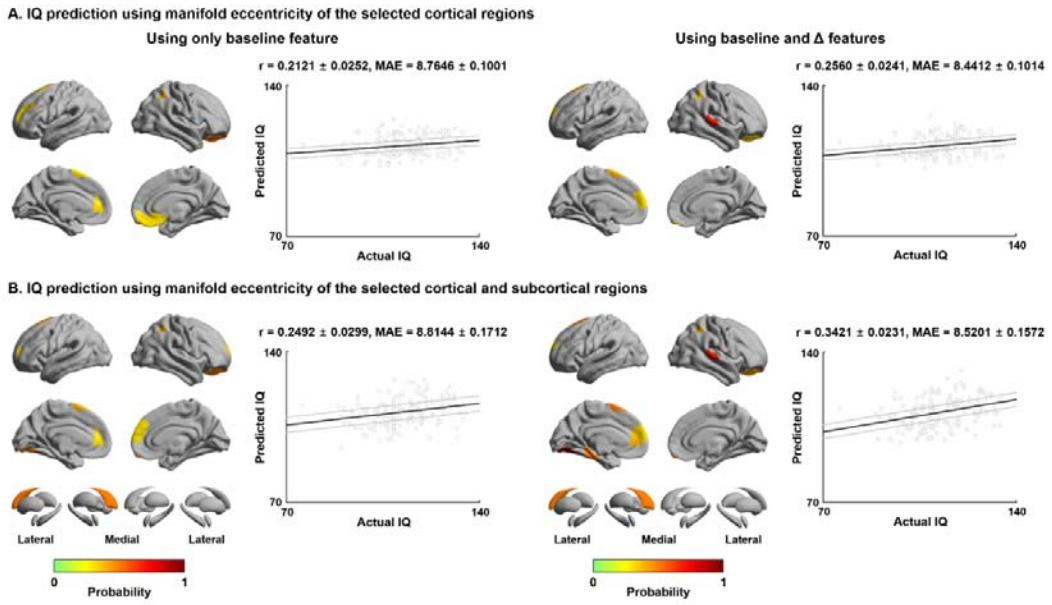

Fig. 6 | IQ prediction. (A) Probability of selected brain regions across ten-fold cross-validation for predicting future IQ using only baseline manifold eccentricity (left), and both baseline and maturational change in the feature (right). Correlations between actual and predicted IQ are reported. Black lines indicate mean correlation and gray lines represent 95% confidence interval for 100 iterations with different training/test dataset. **(B)** The prediction performance when both cortical and subcortical features were considered. *Abbreviations:* IQ, intelligence quotient; MAE, mean absolute error.

Sensitivity analysis

Repeating the longitudinal modeling with a different spatial scale (*i.e.*, 300 parcels), findings were highly consistent (**Fig. S5**). Furthermore, manifold eccentricity of the identified cortical regions and age consistently correlated positively in the different sites and within both biological sexes (**Fig. S6**).

DISCUSSION

The current study explored whole-brain structural connectome maturation from adolescence to young adulthood, based on the application of connectome manifold learning to an accelerated longitudinal imaging cohort [20,60]. We established that higher-order association cortices in prefrontal, medial and superior temporal, as well as parieto-occipital regions expanded in their connectome manifold representation indicative of an increased connectivity differentiation of these areas from the rest of the brain in adolescence. Parallel topological fingerprinting based on graph theory indicated that these changes co-occurred alongside increases of the within-module connectivity of transmodal cortices. Findings were consistent across the different acquisition sites and biological sexes, and similar albeit slightly weaker when correcting connectivity manifolds for MRI-based measures of cortical morphology and microstructure. In addition to cortical manifold expansion, we found a significant strengthening in the cortico-subcortical connectivity of the identified transmodal regions, particularly to the striatum. Decoding of the macroscale findings with *post-mortem* gene expression maps highlighted genes enriched in adolescence and young adulthood in both cortical as well as subcortical targets, supporting our main findings. Finally, cortical and subcortical structural connectome measures were effective in predicting measures of intelligence at follow-up. Collectively, our findings provide new insights into adolescent structural connectome maturation, and how multiple scales of brain organization interact during typical neurodevelopment.

Leveraging advanced manifold learning, we depicted macroscale connectome organization along continuous cortical axes. Similar approaches have previously been harnessed to decompose microstructural [21,45], and functional [10,41–43,48,49,75–77] and dMRI connectomes [51]. These techniques are appealing, as they offer a low dimensional perspective on connectome reconfigurations in a data-driven and spatially unconstrained manner. In our longitudinal study, we could identify marked connectome expansion during adolescence mainly encompassing transmodal and heteromodal association cortex in prefrontal, temporal, and posterior regions, territories that are known to mature late in development [1,2]. Connectome expansion likely indicates an overall greater differentiation of the connectivity of these areas from the rest of the brain, as they would then cover wider portions of the corresponding manifold space. In fact, we observed that manifold expansion in higher-order areas correlated with an increase in their within-module connectivity, but not with participation coefficient and connectivity distance measures that would be more reflective of their between-module connectivity. As such, our findings extend prior dMRI studies that have focussed on specific tract groups and that have indicated considerable developmental shifts in diffusion parameters, such as increases in fractional anisotropy and decreases in mean diffusivity in early and late adolescence [32,78–83]. Other studies have furthermore reported increased streamline count estimates [31]. In this context, our macroscale manifold findings likely reflect an ongoing consolidation of transmodal communities. These findings thus align with prior graph theoretical studies, which have pointed to concurrent increases in network integration and consolidation of network hubs from late childhood to early adulthood [29,30]. Considering their distributed regional substrate, these network effects are likely driven by the ongoing maturation of fiber bundles that interconnect these higher-order cortices, including superior longitudinal fascicules, but also thalamic and basal ganglia pathways [84,85], throughout adolescence.

Projecting manifold solutions back onto cortical surfaces allowed us to integrate our connectome manifold results with morphometric and intracortical intensity indices obtained via structural and quantitative MRI contrasts in the same participants. We were thus able to balance the network level effects against trajectories of intracortical remodeling. Longitudinal changes in these cortical features were overall in agreement with prior work, suggesting marked reductions in cortical thickness in adolescence [1,9], possibly reflecting synaptic pruning processes [86,87] together with decreases in the skewness of intracortical MT profiles, a feature sensitive to preferential myelination of supragranular layers [21]. Although we still observed significant age-related changes in manifold eccentricity after controlling for these intracortical and morphological measures, the effect sizes of our findings were reduced. This effect was particularly evident when running a parallel analysis that additionally controlled for depth dependent shifts in cortical microstructure, a finding in line with more generally demonstrated links between cortical microstructural context and inter-regional connectivity [45,88–90]. In the context of adolescence and prior findings in the NSPN dataset [21], these results thus suggest a coupled process that affects depth-dependent shifts in cortical myeloarchitecture on the one hand, and adolescent shifts in macroscale connectome organization as shown by our longitudinal manifold analyses on the other hand.

In addition to emphasizing a distributed set of association cortices and their cortico-cortical connections, analysis of cortico-subcortical connectivity patterns highlighted the importance of transmodal cortical connectivity to subcortical structures, particularly the striatum. These findings were independently supported by transcriptomic association studies and developmental enrichment analyses, which implicated genes expressed in cortical regions and subcortical structures during late childhood, adolescence, and young adulthood. The striatum has long been recognized to play an important role in mediating large-scale cortical network organization [91–95]. It is known to modulate

activity in prefrontal association areas during memory-driven internal thought processes [96,97], and higher-order cognitive functions, notably motivational processes, decision making, as well as cognitive control and executive functions more generally [97,98]. The striatum also participates in dense cortico-subcortical feedback loops, and exchanges neural activity through dense connections with adjacent basal ganglia structures as well as the thalamus [97,99]. These cortico-subcortical interactions likely involve the interplay of multiple neurotransmitter systems, notably dopaminergic transmission as well as GABAergic inhibitory signaling. On the other hand, perturbations in cortico-striatal connections and atypical GABAergic circuits have been reported in schizophrenia [92], but also other neurodevelopmental conditions such as autism [100,101].

Higher-order cognitive function is likely dependent on overall brain network organization, and its prediction may leverage principles of network integration and segregation that are simultaneously captured in the structural manifold features. Application of a supervised machine learning framework with cross-validation and regularization demonstrated that it is possible to predict inter-individual variations in future IQ from structural connectome manifolds. These findings complement conceptual accounts linking brain organization to cognitive function [41,66,102], and earlier efforts to predict IQ measures from brain network connectivity and graph-based topological indices [12,103–107]. Our evaluations furthermore suggested that predictive performance increased when including both baseline and trajectory data, and when complementing cortical manifold features with subcortical connectivity estimates. These findings reemphasize benefits of incorporating subcortical nodes in the characterization of large-scale cortical network organization and overall cognitive function [108,109].

Adolescence is a time characterized by ongoing brain changes [1–7], increased independence from caregivers, and strong increments in knowledge and our ability to think more abstractly and to cooperate in a more goal directed manner. On the other hand, adolescence is also a sensitive time window for risk taking, the development of addictions, and hosts the onset of several prevalent psychiatric disorders [8–13]. Our study has shown that structural brain network organization continues to mature significantly during this time period, with particularly higher- order association cortices in prefrontal and posterior regions showing an expansion of their corresponding connectome manifold signature. Findings were related to an increased strengthening of intra-community connectivity as well as cortico-subcortical connectivity patterns to striatal regions. Although the current work was restricted to a longitudinal sample of typically developing adolescents, our framework may be useful to explore multi-scale network perturbations in cohorts with a psychiatric diagnosis or those at risk for addiction or atypical neurodevelopment.

METHODS

Participants

We obtained imaging and phenotypic data from the NSPN 2400 cohort, which contains questionnaire data on 2,402 individuals (with MRI data on a subset of ~300) from adolescence to young adulthood in a longitudinal setting [20,60]. Included participants completed quality-controlled (see *Data preprocessing* section) multimodal MRI scans consisting of T1-weighted, MT, and dMRI for at least two time points. Our final sample consisted of a total of 208 subjects (48% female; mean ± SD age = 18.82 ± 2.83 years at baseline and 19.95 ± 2.84 years at follow-up with inter-scan interval of 11.28 ± 1.96 months), collected from three different UK sites: Wolfson Brain Imaging Centre and MRC Cognition and Brain Sciences Unit in Cambridge; and University College London. We divided the participants into a template and non-template cohorts with matched age, sex, and site ratio. The template dataset (n = 30; 50% female; mean ± SD age = 18.69 ± 2.60 years at baseline and 19.84 ± 2.66 at follow-up) was used for constructing template structural connectome manifold and the non-template dataset (n = 178; 47% female; mean ± SD age = 18.84 ± 2.88 years at baseline and 19.97 ± 2.88 at follow-up) was used for conducting main analyses. Of note, changing the template dataset composition did not markedly affect main findings (**Fig. S7**).

MRI acquisition

Imaging data were obtained using a Simens Magnetom TIM Trio 3T scanner. T1-weighted and MT sequences were acquired using a quantitative multiparameter mapping (MPM) sequence (repetition time (TR)/flip angle = 18.7ms/20º for T1-weighted and 23.7ms/6º for MT; six equidistance echo times (TE) = 2.2–14.7ms; voxel size = 1mm^3; 176 slices; field of view (FOV) = 256 × 240mm; matrix size = 256 × 240 × 176) [110]. The dMRI data were acquired using a spin-echo echo-planar imaging (EPI) sequence (TR = 8,700ms; TE = 90ms; flip angle = 90º; voxel size = 2mm^3; 70 slices; FOV = 192 × 192mm^2; matrix size = 96 × 96 × 70; b-value = 1,000s/mm^2; 63 diffusion directions; and 6 b0 images).

Data preprocessing

T1-weighted data were processed using the fusion of neuroimaging preprocessing (FuNP) pipeline integrating AFNI, FSL, FreeSurfer, ANTs, and Workbench [111–116], which is similar to the minimal preprocessing pipeline for the Human Connectome Project [116]. Gradient nonlinearity and b0 distortion correction, non-brain tissue removal, and intensity normalization were performed. Processed data were nonlinearly registered to MNI152 space and white and pial surfaces were generated by following the boundaries between different tissues [113,117–119]. The white and pial surfaces were averaged to generate the midthickness surface, which was used to generate the inflated surface. The spherical surface was registered to the Conte69 template with 164k vertices [120] and downsampled to a 32k vertex mesh. Quality control involved visual inspection of surface reconstruction of T1-weighted data, and cases with faulty cortical segmentation were excluded. Surface-based co-registration between T1-weighted and MT weighted scans were performed. We generated 14 equivolumetric cortical surfaces within the cortex and sampled MT intensity along these surfaces [21]. The vertex-wise MT profiles for each surface depth were averaged based on the Schaefer atlas with 200 parcels [121]. The dMRI data were processed using MRtrix3 [122,123] including correction for susceptibility distortions, head motion, and eddy currents.

Structural connectome manifold identification

Structural connectomes were generated from preprocessed dMRI data [122,123]. Anatomically constrained tractography was performed using different tissue types derived from the T1-weighted image, including cortical and subcortical grey matter, white matter, and cerebrospinal fluid [124].

Multi-shell and multi-tissue response functions were estimated [125] and constrained spherical-deconvolution and intensity normalization were performed [126]. The tractogram was generated with 40 million streamlines, with a maximum tract length of 250 and a fractional anisotropy cutoff of 0.06. Subsequently, spherical-deconvolution informed filtering of tractograms (SIFT2) was applied to reconstruct whole-brain streamlines weighted by the cross-section multipliers, which considers the fiber bundle's total intra-axonal space across its full cross-sectional extent [127]. The structural connectome was built by mapping the reconstructed cross-section streamlines onto the Schaefer 7-network based atlas with 200 parcels [121] then log-transformed to adjust for the scale [128,129].

Cortex-wide structural connectome manifolds were identified using BrainSpace (https://github.com/MICA-MNI/BrainSpace) [42]. First, a template manifold was estimated using a group representative structural connectome of the template dataset. The group representative structural connectome was defined using a distance-dependent thresholding that preserves long-range connections [130]. An affinity matrix was constructed with a kernel of normalized angle and manifolds were estimated via diffusion map embedding (**Fig. 1A**), which is robust to noise and computationally efficient compared to other non-linear manifold learning techniques [131,132]. It is controlled by two parameters α and t, where α controls the influence of the density of sampling points on the manifold ($\alpha = 0$, maximal influence; $\alpha = 1$, no influence) and t controls the scale of eigenvalues of the diffusion operator. We set $\alpha = 0.5$ and $t = 0$ to retain the global relations between data points in the embedded space, following prior applications [10,21,41,42,45]. In this new manifold, interconnected brain regions are closely located and regions with weak inter-connectivity located farther apart. After generating the template manifold, individual-level manifolds were estimated from the non-template dataset and aligned to the template manifold via Procrustes alignment [42]. To analyze the multidimensional manifolds based on a single feature, we simplified the multivariate manifolds into a single scalar value by calculating the Euclidean distance between the center of template manifold and all data points (*i.e.,* brain regions) in the manifold space, which was referred to as manifold eccentricity (**Fig. 1B**) [49]. The template center was defined as the centroid of the first three eigenvectors which explained 50% variance.

Longitudinal modeling for age-related changes in structural manifolds

We assessed longitudinal changes in manifold eccentricity across age using a linear mixed effect model [68], controlling for effects of sex, site, head motion, and subject-specific random intercept to improve model fit in accelerated longitudinal designs. The t-statistics of each brain region were computed and we corrected for multiple comparisons by using a false discovery rate (FDR) threshold of $q < 0.05$ (**Fig. 1C**) [133]. We then calculated Pearson's correlation between mean age and within-subject average in manifold eccentricity for the two time points. The significance of the correlation was assessed using 1,000 permutation tests by randomly shuffling subject indices. A null distribution was constructed, and it was deemed significant if the real correlation value did not belong to the 95% of the distribution (two-tailed $p < 0.05$). We stratified age-related effects based on a seminal model of neural organization and laminar differentiation that contains four cortical hierarchical levels [66] and we calculated Pearson's correlation between age and manifold eccentricity for each level (**Fig. 1D**). We similarly stratified findings with respect to seven intrinsic functional communities [67] (**Fig. 1D**).

Association with connectome topology

We defined clusters within the identified regions based on their spatial boundaries, and associated age with manifold eccentricity for each cluster (**Fig. 2A**). To assess how manifold eccentricity changes related to connectome topology, we calculated degree centrality, as well as modular measures of within-module degree and participation coefficient using the Brain Connectivity Toolbox (https://sites.google.com/site/bctnet/) [70] and connectivity distance using a recently

published approach [77]. Degree centrality is defined as the row-wise sum of the weighted connectivity matrix, representing the connection strength of a given node [70]. Connectivity distance is a given brain region's geodesic distance to its structurally connected brain areas within the cortex [134], and it is defined as the multiplication between the geodesic distance and the binarized structural connectome [10,134]. Within-module degree and participation coefficient are nodal measures reflecting different facets of community organization [70,135–137]. For each individual subject, community structure was defined using Louvain's algorithm [71] and a consistency matrix was constructed, where each element of the matrix represents whether the two different nodes are involved in a same community (*i.e.*, 1) or not (*i.e.*, 0) (**Fig. S1A**). We constructed the group-wise consistency matrix by averaging the consistency matrix of all subjects and applied k-means clustering (**Fig. S1B**). The optimal number of clusters was determined using the silhouette coefficient i.e., the k that maximized the silhouette coefficient [138–142]. We calculated within-module degree and participation coefficient based on these modules. Within-module degree is the degree centrality within a community, indicating intra-community connection strength, while participation coefficient represents inter-community connectivity [70,135–137]. We calculated Pearson's correlations between changes in manifold eccentricity and those in each graph theoretical measure for each cluster (**Fig. 2B**). The significance of the correlation was corrected using 1,000 permutation tests by randomly shuffling subject indices in one of the data vectors, and we corrected for multiple comparisons across clusters using an FDR procedure. To visualize age-related changes in theses parameters, we stratified each measure according to discretized age bins (< 17, 17-19, 19-21, 21-23, ≥ 23; **Fig. S2**).

Cortical morphology and microstructure

It has been shown that cortical morphology and microstructure significantly change during development [1,2,9,21]. Here, we confirmed these changes by assessing age-related longitudinal changes in MRI-based cortical thickness measures and intracortical measures of MT, an index sensitive to myelin content [110,143,144], using linear mixed effect models (**Fig. 3A and S3**) [68]. We further regressed out cortical thickness and MT from the connectome manifold eccentricity metric. We then implemented linear mixed effect models using the residuals of manifold measures, to assess whether age-related connectome manifold effects exist above and beyond age-related effects on cortical morphology and microstructure (**Fig. 3B**).

Transcriptomic analysis

We performed spatial correlation analysis to *post mortem* gene expression data and carried out a developmental enrichment analysis (**Fig. 4**). In brief, we first correlated the t-statistics map, which represents age-related longitudinal changes in manifold eccentricity that controlled for cortical morphology and microstructure, with the *post mortem* gene expression maps provided by the Allen Institute using the Neurovault gene decoding tool [52–54]. Leveraging mixed effect models to associate the input t-statistic map with the genes of six donor brains, Neurovault yields the gene symbols associated with the input spatial map. Gene symbols that passed for a significance level of FDR < 0.05 were further tested whether they are consistently expressed across different donors using abagen toolbox (https://github.com/rmarkello/abagen) [72]. For each gene, we estimated whole-brain gene expression map and correlated it between all pairs of donors. Only genes showing consistent whole-brain expression pattern across donors (FDR < 0.05) were fed into enrichment analysis, which involved comparison against developmental expression profiles from the additional BrainSpan dataset (http://www.brainspan.org) using the cell-type specific expression analysis (CSEA) developmental expression tool (http://genetics.wustl.edu/jdlab/csea- tool-2) [55]. As the Allen Brain Institute repository is composed of adult *post mortem* datasets, it should be noted that the associated gene symbols represent indirect associations with the input t-statistic map derived from the developmental data.

Cortico-subcortical connectivity

For all cortical regions that were identified in the manifold analysis, we assessed their longitudinal changes in streamline strength to several subcortical targets. Specifically, we parcellated the accumbens, amygdala, caudate, hippocampus, pallidum, putamen, and thalamus for each individual [145], and approximated cross-section streamlines. We calculated mean strength of the streamline between each subcortical region and identified cortical regions, and assessed age-related longitudinal changes in the streamline strength using a linear mixed effect model [68], controlling for sex, site, head motion, and subject-specific random intercept. Pearson's correlation between age and streamline strength of the identified subcortical regions was calculated (**Fig. 5A**). For each subcortical region, we stratified the t-statistics and calculated correlation between age and streamline strength (**Fig. 5B**). The significance of the correlation was assessed using 1,000 permutation tests by randomly shuffling subject indices and further corrected for the multiple comparisons using FDR.

Association with the development of cognitive function

Leveraging a supervised machine learning framework with ten-fold cross-validation, we predicted future full IQ score measured by Wechsler Abbreviated Scale of Intelligence [146] using cortical and subcortical features. Four different feature sets were evaluated: (1) manifold eccentricity of the identified cortical regions at baseline and (2) manifold eccentricity at baseline and its longitudinal change (*i.e.*, differences between follow-up and baseline), and (3) cortical manifold eccentricity and streamline strength of the identified subcortical regions at baseline and (4) manifold eccentricity and streamline strength at baseline and their longitudinal changes. For each evaluation, a subset of features that could predict future IQ was identified using elastic net regularization (regularization parameter = 0.5), which shows good performance in feature selection at a given sparsity level compared to L1 (least absolute shrinkage and selection operator)- and L2 (ridge)-norm regularization methods [73]. Feature selection procedure was conducted using the training data (9/10 segments) and it was repeated 10 times with different training and test dataset. The features that were most frequently identified across the cross-validation iterations (>50%) were selected and fed into a linear regression model for predicting IQ scores. Here, the actual feature values were considered, not multiplied by the regression weights. The model was controlled for effects of age, sex, site, and head motion. The IQ prediction using linear regression was performed with a ten-fold cross-validation by training the model with the training data (9/10 segments) and applying it to the test data (1/10 segment). The prediction procedure was repeated 100 times with different training and test sets to reduce bias. Prediction accuracy was indexed by computing Pearson's correlations between the actual and predicted IQ scores as well as mean absolute error (MAE). A 95% confidence interval of the accuracy measures was also reported. Permutation-based correlations across 1,000 tests were conducted by randomly shuffling subject indices to check whether the prediction performance exceeded chance levels.

Sensitivity analysis

a) Spatial scale. To assess the consistency of our findings across spatial scales, we additionally performed the longitudinal modeling using a finer parcellation scheme of 300 parcels (**Fig. S5**) [121].

b) Site effect. Participants were recruited from three different sites. To assess whether the longitudinal changes in manifold eccentricity across age are consistent across different sites, we calculated Pearson's correlation between age and manifold eccentricity of the identified regions (**Fig. S6B**).

c) Sex effect. We repeated the correlation between age and manifold eccentricity for male and

female subjects, separately, to assess whether the age-related changes are affected by sex (**Fig. S6C**).

ACKNOWLEDGMENTS

Dr Bo-yong Park was funded by Molson Neuro-Engineering fellowship by Montreal Neurological Institute and Hospital (MNI) and the Fonds de la Recherche due Québec – Santé (FRQ-S). Dr Richard A. I. Bethlehem was funded by a British Academy Post-Doctoral Fellowship and the Autism Research Trust. Dr Casey Paquola and Dr Raul R. Cruces were funded through postdoctoral fellowships of the FRQ-S. Sara Larivière acknowledges funding from FRQ-S and the Canadian Institutes of Health Research (CIHR). Dr Edward T. Bullmore was supported by a Senior Investigator award from the National Institute of Health Research (NIHR). Dr Boris C. Bernhardt acknowledges research support from the National Science and Engineering Research Council of Canada (NSERC Discovery-1304413), the CIHR (FDN-154298), SickKids Foundation (NI17-039), Azrieli Center for Autism Research (ACAR-TACC), and the Tier-2 Canada Research Chairs program. Drs Bo-yong Park, Richard A. I. Bethlehem, Casey Paquola, and Boris C. Bernhardt are jointly funded through an MNI-Cambridge collaborative award. The Neuroscience and Psychiatry Network (NSPN) study was funded by a Wellcome Trust award to the University of Cambridge and University College London. The data were curated and analyzed using a computational facility funded by an MRC research infra-structure award (MR/M009041/1) and supported by the NIHR Cambridge Biomedical Research Centre. The views expressed are those of the authors and not necessarily those of the NHS, the NIHR or the Department of Health and Social Care.

AUTHOR CONTRIBUTIONS

B.P. and B.C.B. designed the experiments, analyzed the data, and wrote the manuscript. R.A.I.B. aided data curation. R.A.I.B., C.P., S.L., R.R.C., and R.V.D.W. aided with the experiments. E.T.B. designed the NSPN MRI study and edited the manuscript. B.P. and B.C.B. are the corresponding authors of this work and have responsibility for the integrity of the data analysis.

CONFLICT OF INTEREST

The authors declare no conflicts of interest.

REFERENCES

1. Shaw, P. *et al.* Intellectual ability and cortical development in children and adolescents. *Nature* **440**, 676–679 (2006).

2. Gogtay, N. *et al.* Dynamic mapping of human cortical development during childhood through early adulthood. *Proc. Natl. Acad. Sci. U. S. A.* **101**, 8174–8179 (2004).

3. Baum, G. L. *et al.* Development of structure–function coupling in human brain networks during youth. *Proc. Natl. Acad. Sci. U. S. A.* **117**, 771–778 (2020).

4. Dwyer, D. B. *et al.* Large-scale brain network dynamics supporting adolescent cognitive control. *J. Neurosci.* **34**, 14096–14107 (2014).

5. Menon, V. Developmental pathways to functional brain networks: Emerging principles. *Trends Cogn. Sci.* **17**, 627–640 (2013).

6. Kolskår, K. K. *et al.* Key brain network nodes show differential cognitive relevance and developmental trajectories during childhood and adolescence. *eNeuro* **5**, (2018).

7. Larsen, B. & Luna, B. Adolescence as a neurobiological critical period for the development of higher-order cognition. *Neurosci. Biobehav. Rev.* **94**, 179–195 (2018).

8. Stiles, J. Neural Plasticity and Cognitive Development. *Dev. Neuropsychol.* **18**, 237–272 (2000).

9. Khundrakpam, B. S., Lewis, J. D., Kostopoulos, P., Carbonell, F. & Evans, A. C. Cortical Thickness Abnormalities in Autism Spectrum Disorders Through Late Childhood, Adolescence, and Adulthood: A Large-Scale MRI Study. *Cereb. cortex* **27**, 1721–1731 (2017).

10. Hong, S.-J. *et al.* Atypical functional connectome hierarchy in autism. *Nat. Commun.* **10**, 1022 (2019).

11. Michelini, G. *et al.* Atypical functional connectivity in adolescents and adults with persistent and remitted ADHD during a cognitive control task. *Transl. Psychiatry* **9**, (2019).

12. Park, B., Hong, J., Lee, S.-H. & Park, H. Functional connectivity of child and adolescent attention deficit hyperactivity disorder patients: Correlation with IQ. *Front. Hum. Neurosci.* **10**, (2016).

13. Paus, T., Keshavan, M. & Giedd, J. N. Why do many psychiatric disorders emerge during adolescence? *Nat. Rev. Neurosci.* **9**, 947–957 (2008).

14. Giedd, J. N. *et al.* Brain development during childhood and adolescence: A longitudinal MRI study. *Nat. Neurosci.* **10**, 861–863 (1999).

15. Sotiras, A. *et al.* Patterns of coordinated cortical remodeling during adolescence and their associations with functional specialization and evolutionary expansion. *Proc. Natl. Acad. Sci. U. S. A.* **114**, 3527–3532 (2017).

16. Hill, J. *et al.* Similar patterns of cortical expansion during human development and evolution. *Proc. Natl. Acad. Sci. U. S. A.* **107**, 13135–13140 (2010).

17. Tamnes, C. K. *et al.* Development of the cerebral cortex across adolescence: A multisample study of inter-related longitudinal changes in cortical volume, surface area, and thickness. *J. Neurosci.* **37**, 3402–3412 (2017).

18. Raznahan, A., Greenstein, D., Lee, N. R., Clasen, L. S. & Giedd, J. N. Prenatal growth in humans and postnatal brain maturation into late adolescence. *Proc. Natl. Acad. Sci. U. S. A.* **109**, 11366–11371 (2012).

19. Mills, K. L. *et al.* Structural brain development between childhood and adulthood: Convergence across four longitudinal samples. *Neuroimage* **141**, 273–281 (2016).

20. Whitaker, K. J. *et al.* Adolescence is associated with genomically patterned consolidation of the hubs of the human brain connectome. *Proc. Natl. Acad. Sci. U. S. A.* **113**, 9105–9110 (2016).

21. Paquola, C. *et al.* Shifts in myeloarchitecture characterise adolescent development of cortical gradients. *Elife* **8**, 1–23 (2019).

22. Miller, D. J. *et al.* Prolonged myelination in human neocortical evolution. *Proc. Natl. Acad. Sci. U. S. A.* **109**, 16480–16485 (2012).

23. Fair, D. A. *et al.* Functional brain networks develop from a 'local to distributed' organization. *PLoS Comput. Biol.* **5**, 14–23 (2009).

24. Dosenbach, N. U. F. *et al.* Prediction of individual brain maturity using fMRI. *Science (80-.).* **329**, 1358–1361 (2010).

25. Steinbeis, N., Bernhardt, B. C. & Singer, T. Impulse Control and Underlying Functions of the Left DLPFC Mediate Age-Related and Age-Independent Individual Differences in Strategic Social Behavior. *Neuron* **73**, 1040–1051 (2012).

26. Tamnes, C. K., Roalf, D. R., Goddings, A. L. & Lebel, C. Diffusion MRI of white matter microstructure development in childhood and adolescence: Methods, challenges and progress. *Dev. Cogn. Neurosci.* **33**, 161–175 (2018).

27. Schmithorst, V. J. & Yuan, W. White matter development during adolescence as shown by diffusion MRI. *Brain Cogn.* **72**, 16–25 (2010).

28. Lebel, C. & Beaulieu, C. Longitudinal development of human brain wiring continues from childhood into adulthood. *J. Neurosci.* **31**, 10937–10947 (2011).

29. Dennis, E. L. *et al.* Development of brain structural connectivity between ages 12 and 30: A 4-Tesla diffusion imaging study in 439 adolescents and adults. *Neuroimage* **64**, 671–684 (2013).

30. Oldham, S. & Fornito, A. The development of brain network hubs. *Dev. Cogn. Neurosci.* **36**, 100607 (2019).

31. Genc, S. *et al.* Longitudinal white matter development in children is associated with puberty, attentional difficulties, and mental health. *bioRxiv* (2020). doi:10.1101/607671

32. Wierenga, L. M. *et al.* The development of brain network architecture. *Hum. Brain Mapp.* **37**, 717–729 (2016).

33. Baker, S. T. E. *et al.* Developmental changes in brain network hub connectivity in late adolescence. *J. Neurosci.* **35**, 9078–9087 (2015).

34. Chen, Z., Liu, M., Gross, D. W. & Beaulieu, C. Graph theoretical analysis of developmental patterns of the white matter network. *Front. Hum. Neurosci.* **7**, 716 (2013).

35. Fan, Y. *et al.* Brain anatomical networks in early human brain development. *Neuroimage* **54**, 1862–1871 (2011).

36. Grayson, D. S. *et al.* Structural and functional rich club organization of the brain in children and adults. *PLoS One* **9**, e88297 (2014).

37. Grayson, D. S. & Fair, D. A. Development of large-scale functional networks from birth to adulthood: A guide to the neuroimaging literature. *Neuroimage* **160**, 15–31 (2017).

38. Hagmann, P. *et al.* White matter maturation reshapes structural connectivity in the late developing human brain. *Proc. Natl. Acad. Sci. U. S. A.* **107**, 19067–19072 (2010).

39. Khundrakpam, B. S. *et al.* Developmental changes in organization of structural brain networks. *Cereb. Cortex* **23**, 2072–2085 (2013).

40. Nie, J., Li, G. & Shen, D. Development of cortical anatomical properties from early childhood to early adulthood. *Neuroimage* **76**, 216–224 (2013).

41. Margulies, D. S. *et al.* Situating the default-mode network along a principal gradient of macroscale cortical organization. *Proc. Natl. Acad. Sci. U. S. A.* **113**, 12574–12579 (2016).

42. Vos de Wael, R. *et al.* BrainSpace: a toolbox for the analysis of macroscale gradients in neuroimaging and connectomics datasets. *Commun. Biol.* **3**, 103 (2020).

43. Huntenburg, J. M., Bazin, P. L. & Margulies, D. S. Large-Scale Gradients in Human Cortical Organization. *Trends in Cognitive Sciences* **22**, 21–31 (2018).

44. Huntenburg, J. M. *et al.* A Systematic Relationship Between Functional Connectivity and Intracortical Myelin in the Human Cerebral Cortex. *Cereb. cortex* **27**, 981–997 (2017).

45. Paquola, C. *et al.* Microstructural and functional gradients are increasingly dissociated in transmodal cortices. *PLoS Biol.* **17**, e3000284 (2019).

46. Vázquez-Rodríguez, B. *et al.* Gradients of structure–function tethering across neocortex. *Proc. Natl. Acad. Sci. U. S. A.* **116**, 21219–21227 (2019).

47. Karapanagiotidis, T. *et al.* The psychological correlates of distinct neural states occurring during wakeful rest. *bioRxiv* (2020). doi:10.1101/2019.12.21.885772

48. Murphy, C. *et al.* Modes of operation: A topographic neural gradient supporting stimulus dependent and independent cognition. *Neuroimage* **186**, 487–496 (2019).

49. Bethlehem, R. A. I. *et al.* Dispersion of functional gradients across the lifespan. *bioRxiv* (2020). doi:10.1101/2020.02.27.968537

50. Lowe, A. J. *et al.* Targeting age related differences in brain and cognition with multimodal imaging and connectome topography profiling. *Hum. Brain Mapp.* **40**, 5213–5230 (2019).

51. Park, B. *et al.* Connectome and microcircuit models implicate atypical subcortico-cortical interactions in autism pathophysiology. *bioRxiv* (2020). doi:10.1101/2020.05.08.077289

52. Gorgolewski, K. J. *et al.* NeuroVault.Org: A web-based repository for collecting and sharing unthresholded statistical maps of the human brain. *Front. Neuroinform.* **9**, Article 8 (2015).

53. Gorgolewski, K. J. *et al.* Tight fitting genes: finding relations between statistical maps and gene expression patterns. in *F1000Posters* **5**, 1607 (Poster) (2014).

54. Hawrylycz, M. J. *et al.* An anatomically comprehensive atlas of the adult human brain transcriptome. *Nature* **489**, 391–399 (2012).

55. Dougherty, J. D., Schmidt, E. F., Nakajima, M. & Heintz, N. Analytical approaches to RNA profiling data for the identification of genes enriched in specific cells. *Nucleic Acids Res.* **38**,

4218–4230 (2010).

56. Hawrylycz, M. *et al.* Canonical genetic signatures of the adult human brain. *Nat. Neurosci.* **18**, 1832–1844 (2015).

57. Fornito, A., Arnatkevičiūtė, A. & Fulcher, B. D. Bridging the Gap between Connectome and Transcriptome. *Trends Cogn. Sci.* **23**, 34–50 (2019).

58. Altmann, A. *et al.* A systems-level analysis highlights microglial activation as a modifying factor in common forms of human epilepsy. *bioRxiv* 470518 (2018). doi:10.1101/470518

59. Van Den Heuvel, M. P. *et al.* Evolutionary modifications in human brain connectivity associated with schizophrenia. *Brain* **142**, 3991–4002 (2019).

60. Kiddle, B. *et al.* Cohort profile: The NSPN 2400 Cohort: A developmental sample supporting the Wellcome Trust Neuro Science in Psychiatry Network. *Int. J. Epidemiol.* **47**, 18-19g (2018).

61. Louis, T. A., Robins, J., Dockery, D. W., Spiro, A. & Ware, J. H. Explaining discrepancies between longitudinal and cross-sectional models. *J. Chronic Dis.* **39**, 831–839 (1986).

62. Telzer, E. H. *et al.* Methodological considerations for developmental longitudinal fMRI research. *Dev. Cogn. Neurosci.* **33**, 149–160 (2018).

63. McCormick, E. M., Qu, Y. & Telzer, E. H. Activation in context: Differential conclusions drawn from cross-sectional and longitudinal analyses of adolescents' cognitive control-related neural activity. *Front. Hum. Neurosci.* **11**, 141 (2017).

64. McCormick, E. M. & Telzer, E. H. Adaptive Adolescent Flexibility: Neurodevelopment of Decision-making and Learning in a Risky Context. *J. Cogn. Neurosci.* **29**, 413–423 (2017).

65. Crone, E. A. & Elzinga, B. M. Changing brains: how longitudinal functional magnetic resonance imaging studies can inform us about cognitive and social-affective growth trajectories. *Wiley Interdiscip. Rev. Cogn. Sci.* **6**, 53–63 (2015).

66. Mesulam, M. M. From sensation to cognition. *Brain* **121**, 1013–1052 (1998).

67. Yeo, B. T. T. *et al.* The organization of the human cerebral cortex estimated by intrinsic functional connectivity. *J. Neurophysiol.* **106**, 1125–1165 (2011).

68. Worsley, K. J. *et al.* SurfStat: A Matlab toolbox for the statistical analysis of univariate and multivariate surface and volumetric data using linear mixed effects models and random field theory. *Neuroimage* **47**, S102 (2009).

69. Bullmore, E. & Sporns, O. Complex brain networks: graph theoretical analysis of structural and functional systems. *Nat. Neurosci.* **10**, 186–198 (2009).

70. Rubinov, M. & Sporns, O. Complex network measures of brain connectivity: uses and interpretations. *Neuroimage* **52**, 1059–1069 (2010).

71. Blondel, V. D., Guillaume, J. L., Lambiotte, R. & Lefebvre, E. Fast unfolding of communities in large networks. *J. Stat. Mech. Theory Exp.* **2008**, (2008).

72. Arnatkevic iūtė, A., Fulcher, B. D. & Fornito, A. A practical guide to linking brain-wide gene expression and neuroimaging data. *Neuroimage* **189**, 353–367 (2019).

73. Zou, H. & Hastie, T. Regularization and variable selection via the Elastic Net. *J. R. Stat. Soc. Ser. B* **67**, 301–320 (2005).

74. Yarkoni, T., Poldrack, R. A., Nichols, T. E., Van Essen, D. C. & Wager, T. D. Large-scale automated synthesis of human functional neuroimaging data. *Nat. Methods* **8**, 665–670 (2011).

75. Vos De Wael, R. *et al.* Anatomical and microstructural determinants of hippocampal subfield functional connectome embedding. *Proc. Natl. Acad. Sci. U. S. A.* **115**, 10154–10159 (2018).

76. Larivière, S. *et al.* Multiscale Structure–Function Gradients in the Neonatal Connectome. *Cereb. Cortex* (2019). doi:10.1093/cercor/bhz069

77. Larivière, S. *et al.* Functional Connectome Contractions in Temporal Lobe Epilepsy. *bioRxiv* 756494 (2019). doi:10.1101/756494

78. Ashtari, M. *et al.* White matter development during late adolescence in healthy males: A cross-sectional diffusion tensor imaging study. *Neuroimage* **35**, 501–510 (2007).

79. Eluvathingal, T. J., Hasan, K. M., Kramer, L., Fletcher, J. M. & Ewing-Cobbs, L. Quantitative diffusion tensor tractography of association and projection fibers in normally developing children and adolescents. *Cereb. Cortex* **17**, 2760–2768 (2007).

80. Muetzel, R. L. *et al.* The development of corpus callosum microstructure and associations with bimanual task performance in healthy adolescents. *Neuroimage* **39**, 1918–1925 (2008).

81. Olson, E. A. *et al.* White matter integrity predicts delay discounting behavior in 9- to 23-year-olds: A diffusion tensor imaging study. *J. Cogn. Neurosci.* **21**, 1406–1421 (2009).

82. Qiu, D., Tan, L. H., Zhou, K. & Khong, P. L. Diffusion tensor imaging of normal white matter maturation from late childhood to young adulthood: Voxel-wise evaluation of mean diffusivity, fractional anisotropy, radial and axial diffusivities, and correlation with reading development. *Neuroimage* **41**, 223–232 (2008).

83. Snook, L., Paulson, L. A., Roy, D., Phillips, L. & Beaulieu, C. Diffusion tensor imaging of neurodevelopment in children and young adults. *Neuroimage* **26**, 1164–1173 (2005).

84. Bava, S. *et al.* Longitudinal characterization of white matter maturation during adolescence. *Brain Res.* **1327**, 38–46 (2010).

85. Tamnes, C. K. *et al.* Brain maturation in adolescence and young adulthood: Regional age-related changes in cortical thickness and white matter volume and microstructure. *Cereb. Cortex* **20**, 534–548 (2010).

86. Spear, L. P. The adolescent brain and age-related behavioral manifestations. *Neurosci. Biobehav. Rev.* **24**, 417–463 (2000).

87. Petanjek, Z. *et al.* Extraordinary neoteny of synaptic spines in the human prefrontal cortex. *Proc. Natl. Acad. Sci. U. S. A.* **108**, 13281–13286 (2011).

88. Barbas, H. & Rempel-Clower, N. Cortical structure predicts the pattern of corticocortical connections. *Cereb. Cortex* **7**, 635–646 (1997).

89. García-Cabezas, M. Á., Zikopoulos, B. & Barbas, H. The Structural Model: a theory linking connections, plasticity, pathology, development and evolution of the cerebral cortex. *Brain Struct. Funct.* **224**, 985–1008 (2019).

90. Paquola, C. *et al.* A cortical wiring space links cellular architecture, functional dynamics and hierarchies in humans. *bioRxiv* (2020). doi:2020.01.08.899583

91. McCutcheon, R. A., Abi-Dargham, A. & Howes, O. D. Schizophrenia, Dopamine and the

Striatum: From Biology to Symptoms. *Trends Neurosci.* **42**, 205–220 (2019).

92. Tziortzi, A. C. *et al.* Connectivity-based functional analysis of dopamine release in the striatum using diffusion-weighted MRI and positron emission tomography. *Cereb. Cortex* **24**, 1165–1177 (2014).

93. Rieckmann, A., Johnson, K. A., Sperling, R. A., Buckner, R. L. & Hedden, T. Dedifferentiation of caudate functional connectivity and striatal dopamine transporter density predict memory change in normal aging. *Proc. Natl. Acad. Sci. U. S. A.* **115**, 10160–10165 (2018).

94. Hanganu, A., Provost, J. S. & Monchi, O. Neuroimaging studies of striatum in cognition part II: Parkinson's disease. *Front. Syst. Neurosci.* **9**, 138 (2015).

95. Balleine, B. W., Delgado, M. R. & Hikosaka, O. The role of the dorsal striatum in reward and decision-making. *J. Neurosci.* **27**, 8161–8165 (2007).

96. Alexander, G. Parallel Organization of Functionally Segregated Circuits Linking Basal Ganglia and Cortex. *Annu. Rev. Neurosci.* **9**, 357–381 (1986).

97. Aglioti, S. The role of the thalamus and basal ganglia in human cognition. *J. Neurolinguistics* **10**, 255–265 (1997).

98. Graybiel, A. M. Building action repertoires: memory and learning functions of the basal ganglia. *Curr. Opin. Neurobiol.* **5**, 733–741 (1995).

99. Alexander, G. E. & Crutcher, M. D. Functional architecture of basal ganglia circuits: neural substrates of parallel processing. *Trends Neurosci.* **13**, 266–271 (1990).

100. Sohal, V. S. & Rubenstein, J. L. R. Excitation-inhibition balance as a framework for investigating mechanisms in neuropsychiatric disorders. *Mol. Psychiatry* **24**, 1248–1257 (2019).

101. Lee, E., Lee, J. & Kim, E. Excitation/Inhibition Imbalance in Animal Models of Autism Spectrum Disorders. *Biol. Psychiatry* **81**, 838–847 (2017).

102. Crossley, N. A. *et al.* Cognitive relevance of the community structure of the human brain functional coactivation network. *Proc. Natl. Acad. Sci. U. S. A.* **110**, 11583–11588 (2013).

103. Jiang, R. *et al.* Task-induced brain connectivity promotes the detection of individual differences in brain-behavior relationships. *Neuroimage* **207**, 116370 (2020).

104. Greene, A. S., Gao, S., Scheinost, D., Constable, R. T. & Greene, A. Task-induced brain state manipulation improves prediction of individual traits. *Nat. Commun.* **9**, 2807 (2018).

105. Dryburgh, E., McKenna, S. & Rekik, I. Predicting full-scale and verbal intelligence scores from functional Connectomic data in individuals with autism Spectrum disorder. *Brain Imaging Behav.* (2019). doi:10.1007/s11682-019-00111-w

106. Dubois, J., Galdi, P., Paul, L. K. & Adolphs, R. A distributed brain network predicts general intelligence from resting-state human neuroimaging data. *Philos. Trans. R. Soc. B Biol. Sci.* **373**, 20170284 (2018).

107. Van Den Heuvel, M. P., Stam, C. J., Kahn, R. S. & Hulshoff Pol, H. E. Efficiency of functional brain networks and intellectual performance. *J. Neurosci.* **29**, 7619–7624 (2009).

108. Tian, Y., Margulies, D. S., Breakspear, M. & Zalesky, A. Hierarchical organization of the human subcortex unveiled with functional connectivity gradients. *bioRxiv* (2020).

doi:10.1101/2020.01.13.903542

109. Alves, P. N. *et al.* An improved neuroanatomical model of the default-mode network reconciles previous neuroimaging and neuropathological findings. *Commun. Biol.* **2**, 370 (2019).

110. Weiskopf, N. *et al.* Quantitative multi-parameter mapping of R1, PD*, MT, and R2* at 3T: A multi-center validation. *Front. Neurosci.* **7**, 95 (2013).

111. Avants, B. B. *et al.* A reproducible evaluation of ANTs similarity metric performance in brain image registration. *Neuroimage* **54**, 2033–2044 (2011).

112. Cox, R. W. AFNI□: Software for Analysis and Visualization of Functional Magnetic Resonance Neuroimages. *Comput. Biomed. Res.* **29**, 162–173 (1996).

113. Fischl, B. FreeSurfer. *Neuroimage* **62**, 774–781 (2012).

114. Jenkinson, M., Beckmann, C. F., Behrens, T. E. J., Woolrich, M. W. & Smith, S. M. Fsl. *Neuroimage* **62**, 782–790 (2012).

115. Park, B., Byeon, K. & Park, H. FuNP (Fusion of Neuroimaging Preprocessing) Pipelines: A Fully Automated Preprocessing Software for Functional Magnetic Resonance Imaging. *Front. Neuroinform.* **13**, Article 5 (2019).

116. Glasser, M. F. *et al.* The minimal preprocessing pipelines for the Human Connectome Project. *Neuroimage* **80**, 105–124 (2013).

117. Dale, A. M., Fischl, B. & Sereno, M. I. Cortical surface-based analysis: I. Segmentation and surface reconstruction. *Neuroimage* **9**, 179–194 (1999).

118. Fischl, B., Sereno, M. I. & Dale, A. M. Cortical surface-based analysis: II. Inflation, flattening, and a surface-based coordinate system. *Neuroimage* **9**, 195–207 (1999).

119. Fischl, B., Sereno, M. I., Tootell, R. B. H. & Dale, A. M. High-resolution inter-subject averaging and a surface-based coordinate system. *Hum. Brain Mapp.* **8**, 272–284 (1999).

120. Van Essen, D. C., Glasser, M. F., Dierker, D. L., Harwell, J. & Coalson, T. Parcellations and hemispheric asymmetries of human cerebral cortex analyzed on surface-based atlases. *Cereb. cortex* **22**, 2241–2262 (2012).

121. Schaefer, A. *et al.* Local-Global Parcellation of the Human Cerebral Cortex from Intrinsic Functional Connectivity MRI. *Cereb. Cortex* **28**, 3095–3114 (2018).

122. Tournier, J. D. *et al.* MRtrix3: A fast, flexible and open software framework for medical image processing and visualisation. *Neuroimage* **202**, 116137 (2019).

123. Tournier, J. D., Calamante, F. & Connelly, A. MRtrix: Diffusion tractography in crossing fiber regions. *Int. J. Imaging Syst. Technol.* **22**, 53–66 (2012).

124. Smith, R. E., Tournier, J. D., Calamante, F. & Connelly, A. Anatomically-constrained tractography: Improved diffusion MRI streamlines tractography through effective use of anatomical information. *Neuroimage* **62**, 1924–1938 (2012).

125. Christiaens, D. *et al.* Global tractography of multi-shell diffusion-weighted imaging data using a multi-tissue model. *Neuroimage* **123**, 89–101 (2015).

126. Jeurissen, B., Tournier, J. D., Dhollander, T., Connelly, A. & Sijbers, J. Multi-tissue constrained spherical deconvolution for improved analysis of multi-shell diffusion MRI data. *Neuroimage* **103**, 411–426 (2014).

127. Smith, R. E., Tournier, J. D., Calamante, F. & Connelly, A. SIFT2: Enabling dense quantitative assessment of brain white matter connectivity using streamlines tractography. *Neuroimage* **119**, 338–351 (2015).

128. Amico, E. & Goñi, J. Mapping hybrid functional-structural connectivity traits in the human connectome. *Netw. Neurosci.* **2**, 306–322 (2018).

129. Fornito, A., Zalesky, A. & Bullmore, E. *Fundamentals of Brain Network Analysis*. (Academic Press, 2016).

130. Betzel, R. F., Griffa, A., Hagmann, P. & Miši´c, B. Distance-dependent consensus thresholds for generating group-representative structural brain networks. *Netw. Neurosci.* **3**, 475–496 (2019).

131. Tenenbaum, J. B., Silva, V. de & Langford, J. C. A Global Geometric Framework for Nonlinear Dimensionality Reduction. *Science (80-.).* **290**, 2319–2323 (2000).

132. Von Luxburg, U. A tutorial on spectral clustering. *Stat. Comput.* **17**, 395–416 (2007).

133. Benjamini, Y. & Hochberg, Y. Controlling the False Discovery Rate□: A Practical and Powerful Approach to Multiple Testing. *J. R. Stat. Soc.* **57**, 289–300 (1995).

134. Oligschläger, S. *et al.* Gradients of connectivity distance in the cerebral cortex of the macaque monkey. *Brain Struct. Funct.* **224**, 925–935 (2019).

135. Cohen, J. R. & D'Esposito, M. The segregation and integration of distinct brain networks and their relationship to cognition. *J. Neurosci.* **36**, 12083–12094 (2016).

136. Joyce, K. E., Laurienti, P. J., Burdette, J. H. & Hayasaka, S. A new measure of centrality for brain networks. *PLoS One* **5**, (2010).

137. Power, J. D., Schlaggar, B. L., Lessov-Schlaggar, C. N. & Petersen, S. E. Evidence for hubs in human functional brain networks. *Neuron* **79**, 798–813 (2013).

138. Park, B., Tark, K.-J., Shim, W. M. & Park, H. Functional connectivity based parcellation of early visual cortices. *Hum. Brain Mapp.* **39**, 1380–1390 (2018).

139. Bzdok, D. *et al.* Subspecialization in the human posterior medial cortex. *Neuroimage* **106**, 55–71 (2015).

140. Craddock, R. C., James, G. A., Holtzheimer, P. E., Hu, X. P. & Mayberg, H. S. A whole brain fMRI atlas generated via spatially constrained spectral clustering. *Hum. Brain Mapp.* **33**, 1914–1928 (2012).

141. Eickhoff, S. B., Laird, A. R., Fox, P. T., Bzdok, D. & Hensel, L. Functional Segregation of the Human Dorsomedial Prefrontal Cortex. *Cereb. Cortex* **26**, 304–321 (2016).

142. Kannan, S. R., Ramathilagam, S., Sathya, A. & Pandiyarajan, R. Effective fuzzy c-means based kernel function in segmenting medical images. *Comput. Biol. Med.* **40**, 572–579 (2010).

143. Draganski, B. *et al.* Regional specificity of MRI contrast parameter changes in normal ageing revealed by voxel-based quantification (VBQ). *Neuroimage* **55**, 1423–1434 (2011).

144. Helms, G., Dathe, H., Kallenberg, K. & Dechent, P. High-resolution maps of magnetization transfer with inherent correction for RF inhomogeneity and T1 relaxation obtained from 3D FLASH MRI. *Magn. Reson. Med.* **60**, 1396–1407 (2008).

145. Patenaude, B., Smith, S. M., Kennedy, D. N. & Jenkinson, M. A Bayesian model of shape

and appearance for subcortical brain segmentation. *Neuroimage* **56**, 907–922 (2011).

146. Wechsler, D. *Wechsler Abbreviated Scales of Intelligence (WASI)*. (Psychological Corporation, 1999).